

Collective locomotion of two uncoordinated undulatory self-propelled foils ^{EP}

Cite as: Phys. Fluids **33**, 011904 (2021); <https://doi.org/10.1063/5.0036231>

Submitted: 04 November 2020 . Accepted: 24 December 2020 . Published Online: 19 January 2021

 Huiyang Yu (于汇洋),  Xi-Yun Lu (陆夕云), and  Haibo Huang (黄海波)

COLLECTIONS

 This paper was selected as an Editor's Pick



View Online



Export Citation



CrossMark

ARTICLES YOU MAY BE INTERESTED IN

[How to deform an egg yolk? On the study of soft matter deformation in a liquid environment](#)

Physics of Fluids **33**, 011903 (2021); <https://doi.org/10.1063/5.0035314>

[Inertial focusing of elliptical particles and formation of self-organizing trains in a channel flow](#)

Physics of Fluids **33**, 013310 (2021); <https://doi.org/10.1063/5.0035668>

[Collisional ferrohydrodynamics of magnetic fluid droplets on superhydrophobic surfaces](#)

Physics of Fluids **33**, 012012 (2021); <https://doi.org/10.1063/5.0032610>

Physics of Fluids

SPECIAL TOPIC: Tribute to
Frank M. White on his 88th Anniversary

SUBMIT TODAY!

AIP
Publishing

Collective locomotion of two uncoordinated undulatory self-propelled foils

Cite as: Phys. Fluids 33, 011904 (2021); doi: 10.1063/5.0036231

Submitted: 4 November 2020 • Accepted: 24 December 2020 •

Published Online: 19 January 2021



View Online



Export Citation



CrossMark

Huiyang Yu (于汇洋),  Xi-Yun Lu (陆夕云),  and Haibo Huang (黄海波)^{a)} 

AFFILIATIONS

Department of Modern Mechanics, University of Science and Technology of China, Hefei, Anhui 230026, China

^{a)} Author to whom correspondence should be addressed: huanghb@ustc.edu.cn

ABSTRACT

Fish schooling with stable configurations is intriguing. How individuals benefit from hydrodynamic interactions is still an open question. Here, fish are modeled as undulatory self-propelled foils, which is more realistic. The collective locomotion of two foils in a tandem configuration with different amplitude ratios Ar and frequency ratios Fr is considered. Depending on Ar and Fr , the two foils without lateral or yaw motion may spontaneously form stable configurations, separate, or collide with each other. The phase diagram of the locomotion modes in the (Fr, Ar) plane is obtained, which is significantly different from that in Newbolt *et al.* [“Flow interactions between uncoordinated flapping swimmers give rise to group cohesion,” *Proc. Natl. Acad. Sci. U. S. A.* **116**, 2419 (2019)]. For stable configurations, the gap spacing may be almost constant [stable position (SP) mode] or change dynamically and periodically [stable cycle (SC) mode]. In our diagram, the fast SP mode is found. Besides, the border between the separation and SP/SC modes is more realistic. In the fast SP cases, analyses of hydrodynamic force show the phenomenon of inverted drafting, in which the leader achieves hydrodynamic advantages. For the SC mode, the cruising speed increases piecewise linearly with $FrAr$. When $Ar < 1$, the linear slope is identical to that of the isolated leader, and the follower-control mechanism is revealed. Our result sheds some light on fish schooling and predating.

Published under license by AIP Publishing. <https://doi.org/10.1063/5.0036231>

I. INTRODUCTION

Collective motion is ubiquitous in biological and natural systems. Although the invaluable insight into the social traits of collective locomotion, such as schooling and flocking, has been provided by investigations based on experiments and models,¹ several issues about the role of hydrodynamics in collective locomotion are still open questions.^{2–4} One important and intriguing issue is the hydrodynamic advantage. The theoretical research on this issue was first conducted by Weihs *et al.*,^{3,5} who suggested that schooling fish could greatly enhance their thrust production in a diamond configuration using an inviscid potential flow model. However, little biological evidence of hydrodynamic advantage in the diamond pattern has been found.⁴ Due to the difficulty of experimental measures on the energetic savings of schooling, only some limited experimental evidence^{6–8} showed that the individuals can obtain the hydrodynamic advantage of the collective locomotion. The other issue is the role of flows on the emergence of the collective pattern. To investigate this issue, individuals may be modeled as vortex dipoles, flapping foils, and flapping flexible plates.^{9–12} To assess the role of

aero- or hydrodynamics in collective flying and swimming, more quantitative information is needed.^{13,14}

As the simplest model of basic element for schooling, the grouping unit consisting of two individuals in a tandem or side-by-side configuration in uniform flow has been studied by experiments and simulations. The in-line configuration is of particular interest due to its evident hypotaxis between the leader and the follower, which is likely to lead to strong fluid-mediated interaction.¹⁵ For a pair of flexible flags in tandem fixed at the upstream end, Ristroph and Zhang found that the leader, rather than the follower, could benefit from the tandem configuration.¹⁵ The authors referred to this drag reduction as inverted drafting, which is also found in Ref. 16. These results are interpreted with constructive interactions of the two wakes of the tandem bodies creating strong trailing vortices.^{17,18} More similar studies on the performance of two flapping foils are conducted.^{19–22}

In the studies above, the swimmers were held fixed in an oncoming flow and could not propel themselves freely. However, the self-propelled swimmers or flyers in collective locomotion are free to select their speed and relative position through flow-mediated

interactions among them.¹² It is essential to capture this trait in order to understand the role of hydrodynamic interactions on the emergence of the collective pattern.²³ There are numerous studies on the emergence of collective locomotion dynamics in a two-body self-propelled system. Ramanarivo *et al.*²⁴ experimentally studied two synchronized flapping wings in tandem swimming in rotational orbits. The inter-wing spacing is dynamically selected and multiple stable configurations can emerge spontaneously as a result of flow-mediated coupling. It offers an experimental support for the Lighthill conjecture.^{24,25} Zhu *et al.* numerically investigated the flow-mediated interactions among two self-propelled flapping filaments in a tandem configuration.²⁶ Their result showed that multiple stable configurations can be spontaneously formed with the help of the vortex street behind the leader. In the wake, two single (2S) vortices with opposite sign are shed per tail-beat period.²⁷ The follower can enjoy energetic benefits for the cases with the 2S wakes. The propulsive velocity of the school can be enhanced in the compact in-line configuration, but the energetic advantage of the leader was not observed. Some recent studies focus on the group cohesion in schools through high-fidelity simulations.^{28,29} A cohesive group controlled by reinforcement learning is established to exploit the high energy-efficiency state of the following swimmer. With such an active strategy, the following swimmer learns to synchronize with the wake flow of the leader.

In most of the above studies, if active control is not considered, usually two plates are of identical frequency and amplitude. In actual situations, fish may adopt different flapping frequency and amplitude. As far as we know, only Newbolt *et al.* parametrically investigated two flapping tandem hydrofoils with different amplitude and frequency.³⁰ Depending on the amplitude ratio Ar and frequency ratio Fr , the two foils may spontaneously form stable configurations, separate, or collide. A phase diagram for the motion modes is presented. They found that the leader achieves a nearly constant cruising speed as the isolated hydrofoil case, which only depends on its own kinematics. However, the result may be significantly different from the cases of real fish since the simple heaving motions of foils are far from the swimming style of fish. Besides, there is no analysis on thrust and collective advantage.

In this paper, two self-propelled foils in a tandem configuration with different undulatory frequency and amplitude are numerically studied. Our study differs from previous studies in several important ways. First and foremost, our model of undulatory self-propelled foils is more close to the swimming of real fish (see Fig. 1).³¹ However, to maintain the in-line configuration and avoid the utilization of active control, the swimmers are not allowed to yaw or to move laterally.^{10,26,32} The undulatory motion of the hydrofoil

interacting with surrounding fluid leads to the self-propulsion. Second, we mainly focus on flow interactions between two uncoordinated foils with different propulsive capacity. Finally, compared with the experimental studies, our numerical simulations can provide more quantitative information, especially thrust and power, which are crucial to investigate collective advantages. The remainder of this paper is organized as follows: The physical problem and numerical method are presented in Sec. II. Detailed results and relevant mechanisms are discussed in Sec. III, and conclusions are presented in Sec. IV.

II. PROBLEM DESCRIPTION AND METHODOLOGY

In our simulations, two undulatory self-propelled foils in a tandem configuration are considered here, as shown in Fig. 1. A two-dimensional NACA0012 airfoil, a symmetrical airfoil with max thickness 12% at 30% chord, is used to model the geometry of fish.

The kinematic deformation of the foil, i.e., the midline lateral displacement in a local coordinate system, is given by^{33,34}

$$y_i(s, t) = B_i(s) \sin[2\pi(s/L - f_i t)], \quad B_i(s) = A_i \frac{s/L + 0.03125}{1.03125}, \quad (1)$$

where $s \in [0, L]$ is the projected coordinate of the midline on the x axis, L is the projected length of the foil, f is the phase speed, and A is the motion amplitude of the trailing edge. The subscript i in both equations represents the parameters of the leader and follower, respectively. Thus, the deformation of the midline is prescribed over a frame of reference attached to the head of the swimmer. Then, they are transformed into the center of mass frame of reference. The locomotion of each foil is governed by Newton's equations of motion,³⁵ i.e.,

$$m_i \ddot{x}_{c,i} = F_i, \quad \dot{I}_{z,i} \dot{\phi}_{c,i} + I_{z,i} \ddot{\phi}_{c,i} = M_{z,i}. \quad (2)$$

Here, F_i and $M_{z,i}$ are the fluid force and yaw torque acting on the i th foil. $x_{c,i}$ is the position of the center of mass of the body, $\phi_{c,i}$ is the angular velocity, m is the total mass, and $I_{z,i}$ is the moment of inertial about the yaw axis. Except for the validation case, the horizontal movement of the foils is free, while the yaw and lateral locomotion is confined. Therefore, Eq. (2) reduces to

$$m_i \ddot{x}_{c,i} = F_{x,i}. \quad (3)$$

$G(t)$ represents the longitudinal gap spacing between the trailing edge of the leader and the leading edge of the follower. The initial gap spacing is $G_0 = G(t = 0)$.

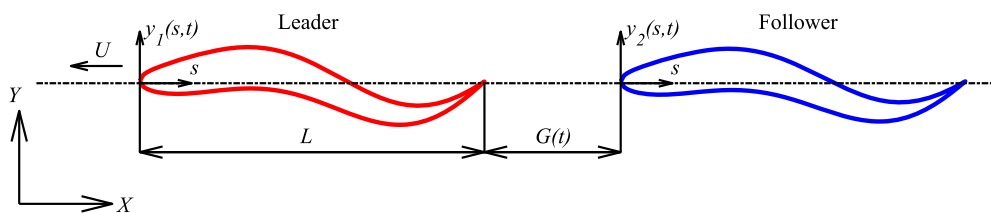


FIG. 1. Sketch of the model for collective locomotion of two undulatory foils in tandem.

The fluid flow is governed by the incompressible Navier–Stokes equations

$$\frac{\partial \mathbf{v}}{\partial t} + \mathbf{v} \cdot \nabla \mathbf{v} = -\frac{1}{\rho} \nabla p + \nu \nabla^2 \mathbf{v} + \mathbf{f}_b, \quad (4)$$

$$\nabla \cdot \mathbf{v} = 0, \quad (5)$$

where \mathbf{v} is velocity, p is pressure, ρ the density of the fluid, and ν is the fluid kinematic viscosity.³⁶ The Navier–Stokes equation is solved by the immersed boundary-lattice Boltzmann method (IB-LBM).³⁷ In the scheme, the immersed boundary is discretized into many Lagrangian points. The body force term \mathbf{f}_b in Eq. (4) represents an interaction force between the fluid and the immersed boundary to enforce the no-slip velocity boundary condition. A detail description of the numerical method can be found in Refs. 38 and 39.

The computational domain for fluid flow is chosen as $[-15, 30] \times [-15, 15]$ in the x and y directions, respectively. The center of mass of the leading foil is initially located at $(0, 0)$. A constant pressure with $\mathbf{v} = 0$ is imposed at all boundaries, while $\partial \mathbf{v} / \partial x = 0$ with constant pressure is set for the outlet.⁴¹ The initial condition is $\mathbf{v} = 0$ in the whole flow field. A uniform mesh with $\Delta x = \Delta y = 0.0075L$ and the time step $\Delta t = 0.0001T_p$ are adopted in the simulations. $T_p = 1/f_1$ is the tail-beat period of the swimmer or that of the leader in the tandem case.

To validate the present numerical method and check the temporal and spatial resolutions, two cases of a single undulatory foil are simulated. Figure 2(a) shows the lift and drag coefficient in the case of $Re_U = UL/\nu = 5000$. Figure 2(b) shows the propulsive velocity of the isolated undulatory foil in cases of $Re = 500, 1000$. In this case, besides the longitudinal locomotion, the self-propelled swimmer can yaw and move laterally. It is seen that all the results agree well with those in Refs. 27 and 40.

The dimensionless governing parameters are listed as follows: the Reynolds number $Re = 2\pi A_1 f_1 L/\nu$,²⁷ the amplitude ratio $Ar = A_2/A_1$, the frequency ratio $Fr = f_2/f_1$, the density ratio $M = \rho_s/\rho$, and the initial longitudinal spacing G_0 . The characteristic quantities ρ , L , and U_{ref} are chosen as the reference density, length, and velocity. $U_{ref} = L/T_p$ is the characteristic velocity.

III. RESULTS AND DISCUSSION

The collective motions of two undulatory self-propelled foils in tandem were simulated. We focused on the effects of

Ar ($Ar \in [0, 2]$) and Fr ($Fr \in [0, 2]$). In the simulations, $Re = 2000$, $M = 1.0$, $A_1 = 0.125$, and $f_1 = 0.1$ are fixed. Therefore, the undulatory motion of the leading foil is unchanged.

A series of cases with different Fr and Ar were simulated. We found that depending on Fr and Ar , the two foils may spontaneously form stable configurations, separate, or collide with each other. For stable configurations, the equilibrium gap spacing G^{eq} may be constant [stable position (SP) mode] or changes periodically [stable cycle (SC) mode]. In the SP and SC modes, the two foils form a school that travels together, while both the separation and collision modes imply the failure of the collective behavior.

The phase diagram of the locomotion modes in the (Fr, Ar) plane is shown in Fig. 3(a). When the follower is underdriven, e.g., $Fr = 0.9$ and $Ar = 0.9$, even initially the follower is very close to the leader, e.g., $G_0 = 0.1$, finally the follower may separate with the leading one [see Fig. 3(b)]. When the follower is overdriven, e.g., $Fr = 1.7$ and $Ar = 0.9$, even initially $G_0 = 6.1$, the follower may still collide with the leader [$G_0 = 1.1$ shown in Fig. 3(b)]. The separation and collision modes occur when $FrAr$ is small and large, respectively.

The SC and SP modes emerge at moderate Ar and Fr ; especially, the SP mode only appears at $Fr = 1$ [see Fig. 3(a)]. These modes appear because at moderate Ar and Fr , the propulsive capacity of the two individuals is comparable. In the SP mode ($Fr = 1$), the two foils are in-phase and the undulatory motions are of the same frequency. If Ar is not too larger, e.g., $Ar = 0.9$, at the equilibrium state, the gap spacing between the two foils is almost constant [$G^{eq} \approx 1.7$ in Fig. 3(b)]. The school travels approximately as fast as the isolated foil. It is the slow SP mode.

When approximately $Fr^{1.7} Ar \geq 1$ and $Fr \neq 1$, the SC mode would appear [see Fig. 3(a)]. For example, in the case $Fr = 1.1$ and $Ar = 0.9$, the gap spacing G^{eq} would change periodically [see Fig. 3(b)]. It is mainly triggered by the nonuniform undulatory frequency. The follower is periodically captured by the vortex wake of the leader [see Fig. 4 (Multimedia view)]. In the SC cases ($Fr \neq 1$), the initial phase difference between the two foils is not important because the phase difference would change continuously during the travel.

In the slow SP mode ($Ar < 1.4$), there may be several discrete stable positions behind the leader, which depends on Ar and G_0 .³⁰ For example, in the case of $Ar = 1$, at equilibrium states, G^{eq} are 0.45 and 0.9, respectively, for the cases of $G_0 = 0.1$ and $G_0 = 1.0$ [see Fig. 5(b)]. The normalized cruising speed \bar{U}/\bar{U}_α as a function of

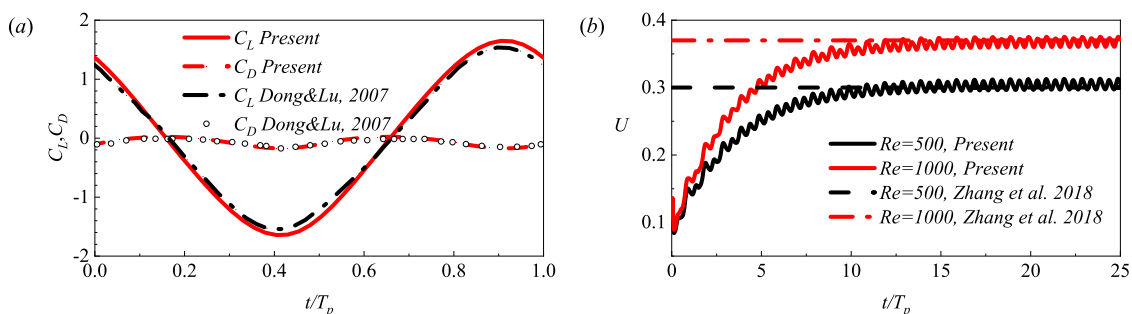


FIG. 2. Validation for the case of (a) flow over a single traveling wavy foil at $Re_U = 5000$ and (b) propulsive velocity of a single self-propelled undulatory foil. The details of two cases can be referred to Refs. 27 and 40, respectively.

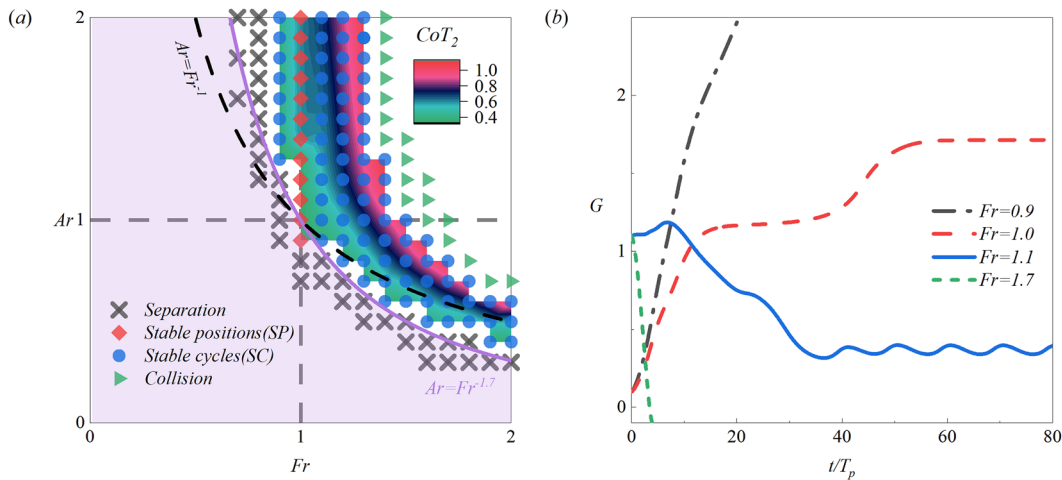


FIG. 3. (a) Phase diagram in the (Fr, Ar) plane. Each point in the plane represents a case we simulated. The purple solid ($Ar = Fr^{-1.7}$) and black dashed ($Ar = Fr^{-1}$) lines approximately denote the borders between the separation and SP/SC modes in our study and Ref. 30, respectively. The cost of transport (CoT) of the follower is also plotted in the SP/SC region. (b) Typical evolutions of gap spacing G for separation ($Fr = 0.9$), SP ($Fr = 1.0$), SC ($Fr = 1.1$), and collision ($Fr = 1.7$) modes. In all these cases, $Ar = 0.9$.

Ar is shown in Fig. 5(a), where the subscript α denotes the case of an isolated leading foil. It is seen that under the above cases, the speed is about 1.1 and 1.03, respectively. As Ar increases to 1.4, \bar{U}/\bar{U}_α increases dramatically to 1.36. Meanwhile, G^{eq} is very small [see Fig. 5(b)]. Therefore, in the mode, the school is compact and travels fast,²³ which is referred to as the fast SP mode.

Our phase diagram is partially consistent with that in Ref. 30, e.g., the approximate distribution of the separation and collision modes. However, there are several significant differences. First, in our phase diagram, there is the fast SP mode, which did not appear in Ref. 30. The fast SP mode indeed was found in Ref. 24. On the other hand, although the unstable position mode is found in Ref. 30 for two rigid heaving foils, there is no biological evidence to support it. Second, in our phase diagram, the border between the separation mode and the SP/SC mode may be more realistic because now the SC mode includes the cases of $Fr = 0.9$, which have been observed in the experiment of Ref. 42. This partially supports the correctness of our phase diagram. The features are all attributed to the more realistic swimmer model that we used. From the phase diagram, we can get some inspiration. It is seen that the range of Fr for the SC mode

is not too wide, e.g., for cases of $Ar = 1$, the range is $Fr \in [1, 1.6)$. The dynamic equilibrium of the school is relatively fragile. Under the circumstances of comparable size, the predators may increase the frequency to shift to the collision mode quickly and optimize their hunting process. On the other hand, the prey also adopts the strategy of high-frequency motions, i.e., enhancing f_1 to decrease Fr . In the way, the prey can escape from predators, i.e., exploiting the separation mode.

The mechanical and propulsive properties of the foils are further investigated. The propulsive performance of the foils is quantified by the mean propulsive speed \bar{U} , thrust coefficient C_T , effective force coefficient C_{eff} , and the cost of transport CoT . They are defined as follows:^{11,29,43}

$$\bar{U} = \frac{1}{U_{ref}T} \int_{t'}^{t'+T} U(t) dt, \quad C_T(s) = \frac{2\bar{F}_T}{\rho U_{ref}^2 L}, \quad (6)$$

$$C_{eff}(s) = \frac{2\bar{F}_{eff}}{\rho U_{ref}^2 L}, \quad CoT = \frac{\bar{P}}{M\bar{U}},$$

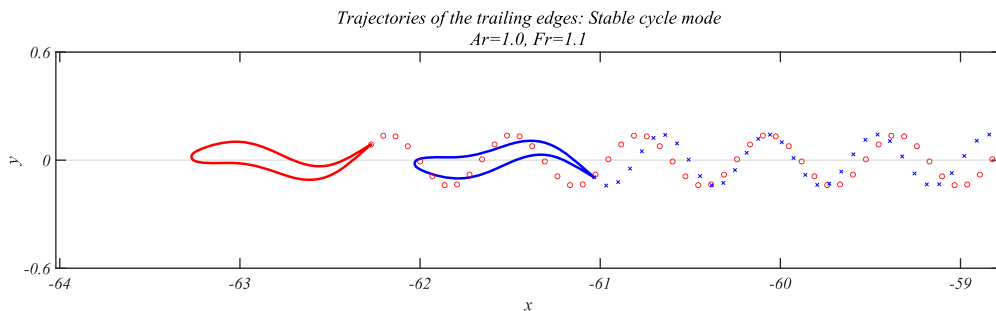


FIG. 4. Trajectories of the trailing edges for the SC mode ($Ar = 1$ and $Fr = 1.1$). Multimedia view: <https://doi.org/10.1063/5.0036231.1>

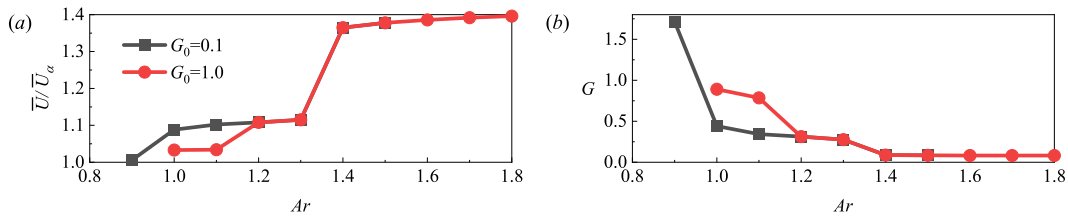


FIG. 5. In the SP mode ($Fr = 1$), the normalized mean propulsive speed of the school (a) and the longitudinal gap spacing G (b) as functions of Ar . The effect of G_0 is presented.

where $P(t) = \sum_s F_{eff} U$. The overbar denotes temporal averaging over an undulatory period T . F_T and F_{eff} are

$$F_T(s, t) = \frac{1}{2U} \int_{B(s)} (P_L(r, t) + |P_L(r, t)|) dr,$$

$$F_{eff}(s, t) = \frac{1}{U} \int_{B(s)} P_L(r, t) dr,$$
(7)

where $P_L(r, t) = \mathbf{F}_L(r, t) \cdot \frac{\partial \mathbf{X}(r, t)}{\partial t}$. \mathbf{F}_L represents the distributed force acting on the Lagrangian points by the surrounding fluid. $\frac{\partial \mathbf{X}(r, t)}{\partial t}$ denotes the velocity of the Lagrangian points. For a steady swimming process, the time-averaged force over the cycle is zero.²³ Thus, by calculating the projection of force in the direction of velocity, the instantaneous forces are determined.²⁹ The drag force $C_D(s)$ on a segment of the foil is

$$C_D(s) = C_T(s) - C_{eff}(s).$$
(8)

Here, the foil is divided into ten equal discrete segments along the midline. The force is calculated on each segment's upper and lower surface, i.e., $B(s)$.

In order to explore the hydrodynamic advantages of the SP mode, the thrust and effective force coefficient along the body are shown in Figs. 6(a) and 6(b). The cases of $Ar = 0.9$ and 1.2 are in the slow SP mode and $Ar = 1.5$ is in the fast SP mode. In most cases, the majority of the thrust is produced by the rear part of the body. This result is consistent with those from theory and experiment.^{44,45}

In all cases of the slow SP mode, C_T and C_{eff} of the leading foils are almost identical.²⁶ Here, we focus on the performance of the follower. For the $Ar = 0.9$ case, although the follower is underdriven, the front part of the follower can generate significant thrust. Therefore, in the case, the underdriven follower can benefit from the leader through the wake–structure interaction. For the cases with a larger Ar , e.g., $Ar = 1.2$, C_T at the rear part of the follower is enhanced and C_{eff} at its front part decreases. Thus, the C_D would increase, and the overdriven follower is suppressed in the case.

In the fast SP mode, e.g., the case of $Ar = 1.5$, two foils are very close, and the leading foil may get hydrodynamic advantage.⁴⁶ Our result shows that the time-averaged drag force experienced by the leader is smaller than that of the follower. Specifically, the drag coefficients for the leader and follower are $C_{D1} = 0.0284$ and $C_{D2} = 0.0412$, respectively. This drag reduction of the leader is analogous to the inverted drafting.¹⁵ A smaller drag force is favorable for the leader to cruise with higher speed. Then, the two foils may swim faster than the single foil case. The fast SP mode presents a more magnificent image of motherhood (a mother pushes her calf forward) rather than the predator–prey relation.

The instantaneous vorticity contours for the slow and fast SP modes are shown in Figs. 7(a) and 7(b), respectively. For the slow mode (the case of $Ar = 0.9$), a 2S wake is shed behind the leader. The follower swims through the cores of positive and negative vortices alternatively. By moving with the local lateral flow, the weak follower can keep pace with the leader. For the fast SP mode (the case of $Ar = 1.5$), the two foils are so close that the leader's trailing edge vortex

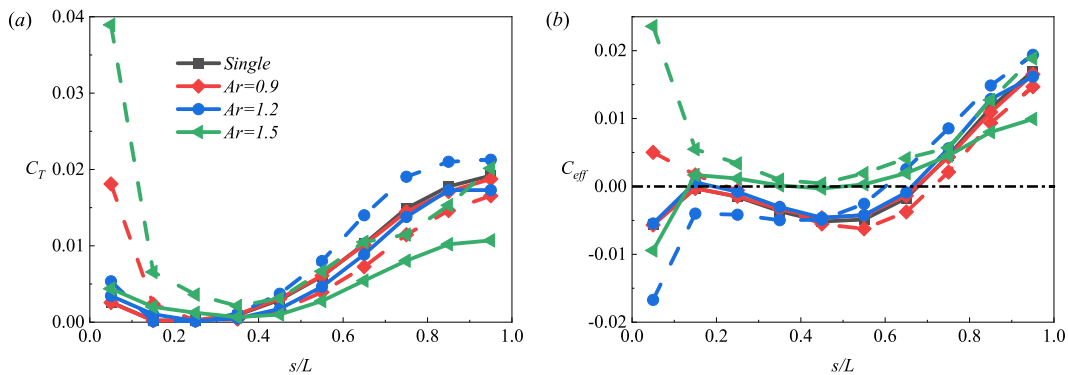


FIG. 6. Hydrodynamic performance of typical cases of the SP mode: (a) thrust coefficient and (b) effective force coefficient along the body. The solid and dashed lines denote the curves of the leader and follower, respectively.

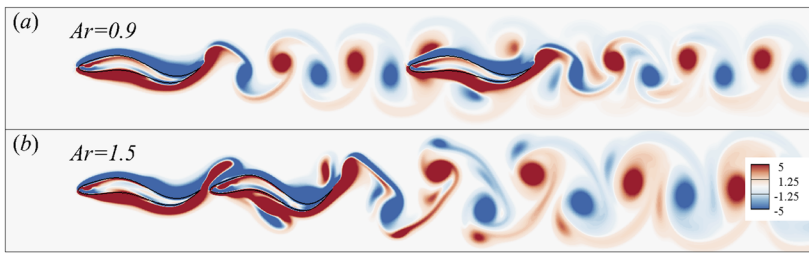


FIG. 7. Typical instantaneous vorticity contours of the SP mode at $t/T_p = 0$ in (a) the slow ($Ar = 0.9$) and (b) fast ($Ar = 1.5$) modes.

(TEV) dissipates quickly. On the other hand, the leader's leading-edge vortex (LEV) is captured by the follower and merges with that of the follower. The merged LEV is finally shed from the follower as the TEV. In this way, the two tandem foils undulate like a longer single swimmer, and the propulsive capacity improves significantly.

For the SC mode, at the equilibrium state, G^{eq} and U change periodically. The scaled mean cruising speed \bar{U}/Fr as functions of Ar in the SC mode is shown in Fig. 8(a). It is seen that the curve can be approximately divided into two segments, and for both segments, \bar{U}/Fr is proportional to Ar .

When Fr is close to unity, e.g., $Fr = 1.1$, the performance should be close to that of the SP mode (cases of $Fr = 1$). The difference is that the gap spacing between the two foils changes periodically in the cases of $Fr = 1.1$ (the SC mode). It is easy to imagine that when the follower is closer to or far away from the leader, the SC cases periodically switch between the compact and sparse configurations. Hence, the overall performance should be between those of the fast and slow SP modes. In the region of $Ar > 1$ [see Fig. 8(a)], \bar{U}/Fr of the fast and slow SP modes are also plotted for comparison. We can see that when Fr is close to unity, \bar{U}/Fr is between those of the fast and slow SP modes.

When Fr is larger ($Ar < 1$), the slope of the scaled lines in Fig. 8(a) is about $k = 0.58$. In the following, we would explain why the slope is 0.58. First, the thrust force would be analyzed to elucidate the feature of the cases with large Fr . The normalized thrust coefficient $C_T^* = 2\bar{F}_T/\rho f_2^2 L^3$ for cases with different Fr ($1.3 \leq Fr \leq 1.8$) but identical Ar ($Ar = 0.7$) are shown in Fig. 8(b). It is seen that the

follower is overdriven in all cases due to the large C_T^* , especially in the front and rear part of the foil. Besides, in the cases of $Fr \geq 1.5$, the distribution curves of C_T^* along the leader's body approximately collapse into a single curve. It seems that $C_T^* \propto \bar{F}_T/f_2^2$ is a constant in the cases of high Fr . In other words, the thrust force experienced by the leader is determined by the follower's undulatory frequency ($\bar{F}_T \propto f_2^2$). Hence, in the cases of high Fr , the follower dominates the school's collective locomotion. Because in the SC mode, G^{eq} is adjustable, it seems that through changing Fr , e.g., $Fr > 1.4$, the follower could dominate the collective behavior of the school and reach any desired position.³⁰

Second, the cruising speed of a swimmer \bar{U} is directly correlated with the model of the swimmer and the flapping pattern, i.e., the cruising Reynolds number $Re_U = \frac{\bar{U}L}{\nu}$ is proportional to the transverse Reynolds number $Re = \frac{2\pi A_1 f_1 L}{\nu}$ by⁴⁷

$$Re_U = \lambda Re. \tag{9}$$

Hence, we have $\bar{U}_\alpha = \lambda(2\pi A_1 f_1)$ for an isolated leader. The coefficient λ is a constant for a specified isolated swimmer with a specified flapping (undulatory) pattern. When Fr is large, the follower dominates the collective behavior. Therefore, the cruising speed of the two tandem swimmers \bar{U} is determined by the follower $\bar{U} = \lambda(2\pi A_2 f_2)$. Then, we have, $\bar{U} = \frac{\bar{U}_\alpha}{2\pi A_1 f_1} 2\pi A_2 f_2 = \bar{U}_\alpha Fr Ar$. In our cases, $\bar{U}_\alpha = 0.58$. Hence, in the region of $Ar < 1$, the slope of the collapsed lines is $k = \frac{\Delta(\bar{U}/Fr)}{\Delta Ar} = 0.58$ [see Fig. 8(a)], where Δ means

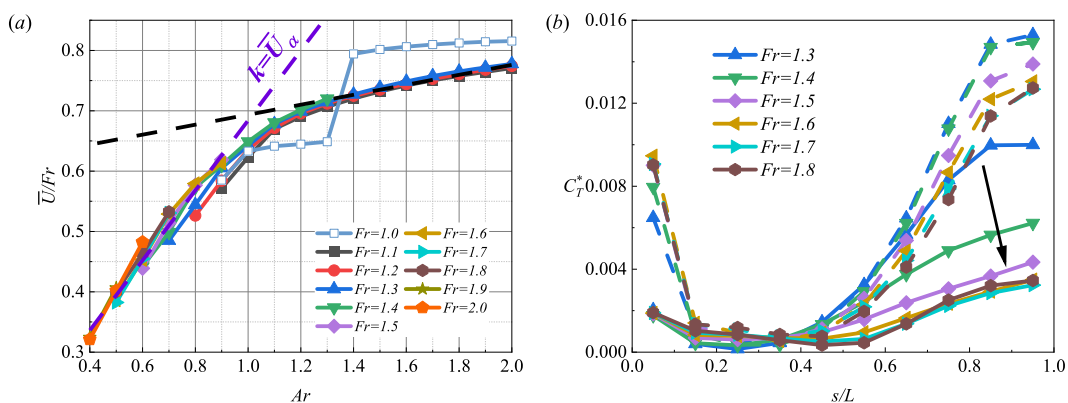


FIG. 8. Rescaled propulsive speed (a) and thrust coefficient (b) of the undulatory foils in the cases with different Fr ($1.3 \leq Fr \leq 1.8$) but identical Ar ($Ar = 0.7$). The solid and dashed lines denote the curves of the leader and follower, respectively.

the a small variation in the parameter. Furthermore, the proportional relationship shown in Eq. (9) is identical to that in Ref. 47, which is proposed for biological propulsion at a high Reynolds number. Therefore, $Re = 2000$ is sufficient to characterize the real fish swimming.

The contours of CoT of the trailing swimmer are also plotted in the phase diagram [see Fig. 3(a)]. It is seen that the follower in the SP/SC mode achieves the lowest CoT near the border between the separation and SP/SC modes. In other words, the “lazy” follower, which is underdriven, consumes the least energy to keep up with the leader. On the other hand, the “lazy” follower also has a risk of departing from the leader because it is so close to the separation mode. It is also seen that the CoT increases with $FrAr$, i.e., the propulsive capacity of the follower, resulting in the enhancement of \bar{U} .

IV. CONCLUSIONS

The collective locomotion of a pair of tandem uncoordinated foils with different Ar and Fr is investigated numerically. The school may spontaneously form SP/SC, separation, or collision modes. Our phase diagram is partially consistent with that in Ref. 30 with several significant differences. In our diagram, first, the fast SP mode is found. Second, the border between separation and the SP/SC mode is more realistic. The features are all attributed to the more realistic swimmer model that we used. From the phase diagram, we also get some inspiration, such as the rationale behind the high-frequency undulatory motions of both predators and the prey, advantage, and risk of the “lazy” follower.

In the study of uncoordinated tandem swimmers, instead of focusing on the wake–follower interaction, here, we pay more attention to the follower–control mechanism. In the fast SP mode ($Fr = 1$, $Ar > 1.4$), due to the mechanism, inverted drafting is found. In the SC mode, in the region of $Ar < 1$, due to the mechanism, the collective locomotion is wholly controlled by the follower. Specifically, \bar{U}/Fr is a linear function of Ar , and the slope of 0.58 is identical to that of a single foil (the leader). The result may further enrich the category of the hydrodynamic advantage of aquatic collective behaviors.

ACKNOWLEDGMENTS

This work was supported by the Natural Science Foundation of China (NSFC) (Grant Nos. 11872064, 11621202, and 11972342).

DATA AVAILABILITY

The data that support the findings of this study are available from the corresponding author upon reasonable request.

REFERENCES

- ¹I. D. Couzin, J. Krause, N. R. Franks, and S. A. Levin, “Effective leadership and decision-making in animal groups on the move,” *Nature* **433**, 513 (2005).
- ²M. Daghooghi and I. Borazjani, “The hydrodynamic advantages of synchronized swimming in a rectangular pattern,” *Bioinspiration Biomimetics* **10**, 056018 (2015).
- ³D. Weihs, “Hydromechanics of fish schooling,” *Nature* **241**, 290 (1973).
- ⁴B. L. Partridge and T. J. Pitcher, “Evidence against a hydrodynamic function for fish schools,” *Nature* **279**, 418 (1979).
- ⁵D. Weihs, “Some hydrodynamical aspects of fish schooling,” in *Swimming and Flying in Nature* (Springer, 1975), pp. 703–718.
- ⁶S. S. Killen, S. Marras, J. F. Steffensen, and D. J. McKenzie, “Aerobic capacity influences the spatial position of individuals within fish schools,” *Proc. R. Soc. B* **279**, 357 (2012).
- ⁷S. J. Portugal, T. Y. Hubel, J. Fritz, S. Heese, D. Trobe, B. Voelkl, S. Hailes, A. M. Wilson, and J. R. Usherwood, “Upwash exploitation and downwash avoidance by flap phasing in ibis formation flight,” *Nature* **505**, 399 (2014).
- ⁸I. Ashraf, H. Bradshaw, T.-T. Ha, J. Halloy, R. Godoy-Diana, and B. Thiria, “Simple phalanx pattern leads to energy saving in cohesive fish schooling,” *Proc. Natl. Acad. Sci. U. S. A.* **114**, 9599 (2017).
- ⁹M. Gazzola, A. A. Tchieu, D. Alexeev, A. de Brauer, and P. Koumoutsakos, “Learning to school in the presence of hydrodynamic interactions,” *J. Fluid Mech.* **789**, 726 (2016).
- ¹⁰Z.-R. Peng, H. Huang, and X.-Y. Lu, “Hydrodynamic schooling of multiple self-propelled flapping plates,” *J. Fluid Mech.* **853**, 587 (2018).
- ¹¹X. Lin, J. Wu, T. Zhang, and L. Yang, “Phase difference effect on collective locomotion of two tandem autopropelled flapping foils,” *Phys. Rev. Fluids* **4**, 054101 (2019).
- ¹²N. Taketoshi, T. Omori, and T. Ishikawa, “Elasto-hydrodynamic interaction of two swimming spermatozoa,” *Phys. Fluids* **32**, 101901 (2020).
- ¹³F. E. Fish and G. V. Lauder, “Passive and active flow control by swimming fishes and mammals,” *Annu. Rev. Fluid Mech.* **38**, 193 (2006).
- ¹⁴Y. Zhang, J. Han, and G. Chen, “Effects of the flapping frequency on the thrust performance for three-dimensional bionic multi-wings in a schooling,” *Phys. Fluids* **31**, 117110 (2019).
- ¹⁵L. Ristroph and J. Zhang, “Anomalous hydrodynamic drafting of interacting flapping flags,” *Phys. Rev. Lett.* **101**, 194502 (2008).
- ¹⁶J. Deng, X.-M. Shao, and Z.-S. Yu, “Hydrodynamic studies on two traveling wavy foils in tandem arrangement,” *Phys. Fluids* **19**, 113104 (2007).
- ¹⁷S. Alben, “Wake-mediated synchronization and drafting in coupled flags,” *J. Fluid Mech.* **641**, 489 (2009).
- ¹⁸M. J. Shelley and J. Zhang, “Flapping and bending bodies interacting with fluid flows,” *Annu. Rev. Fluid Mech.* **43**, 449 (2011).
- ¹⁹B. M. Boschitsch, P. A. Dewey, and A. J. Smits, “Propulsive performance of unsteady tandem hydrofoils in an in-line configuration,” *Phys. Fluids* **26**, 051901 (2014).
- ²⁰T. M. Broering, Y. Lian, and W. Henshaw, “Numerical investigation of energy extraction in a tandem flapping wing configuration,” *AIAA J.* **50**, 2295 (2012).
- ²¹Y. Bao and J. J. Tao, “Dynamic reactions of a free-pitching foil to the reverse Kármán vortices,” *Phys. Fluids* **26**, 031704 (2014).
- ²²L. Cong, B. Teng, and L. Cheng, “Hydrodynamic behavior of two-dimensional tandem-arranged flapping flexible foils in uniform flow,” *Phys. Fluids* **32**, 021903 (2020).
- ²³Z.-R. Peng, H. Huang, and X.-Y. Lu, “Collective locomotion of two closely spaced self-propelled flapping plates,” *J. Fluid Mech.* **849**, 1068 (2018).
- ²⁴S. Ramananarivo, F. Fang, A. Oza, J. Zhang, and L. Ristroph, “Flow interactions lead to orderly formations of flapping wings in forward flight,” *Phys. Rev. Fluids* **1**, 071201 (2016).
- ²⁵M. J. Lighthill, *Mathematical Biofluidynamics* (SIAM, 1975).
- ²⁶X. Zhu, G. He, and X. Zhang, “Flow-mediated interactions between two self-propelled flapping filaments in tandem configuration,” *Phys. Rev. Lett.* **113**, 238105 (2014).
- ²⁷D. Zhang, G. Pan, L. Chao, and Y. Zhang, “Effects of Reynolds number and thickness on an undulatory self-propelled foil,” *Phys. Fluids* **30**, 071902 (2018).
- ²⁸G. Novati, S. Verma, D. Alexeev, D. Rossinelli, W. M. Van Rees, and P. Koumoutsakos, “Synchronisation through learning for two self-propelled swimmers,” *Bioinspiration Biomimetics* **12**, 036001 (2017).
- ²⁹S. Verma, G. Novati, and P. Koumoutsakos, “Efficient collective swimming by harnessing vortices through deep reinforcement learning,” *Proc. Natl. Acad. Sci. U. S. A.* **115**, 5849 (2018).

- ³⁰J. W. Newbolt, J. Zhang, and L. Ristroph, “Flow interactions between uncoordinated flapping swimmers give rise to group cohesion,” *Proc. Natl. Acad. Sci. U. S. A.* **116**, 2419 (2019).
- ³¹N. Thekkethil, A. Sharma, and A. Agrawal, “Unified hydrodynamics study for various types of fishes-like undulating rigid hydrofoil in a free stream flow,” *Phys. Fluids* **30**, 077107 (2018).
- ³²Z.-R. Peng, H. Huang, and X.-Y. Lu, “Collective locomotion of two self-propelled flapping plates with different propulsive capacities,” *Phys. Fluids* **30**, 111901 (2018).
- ³³J. Carling, T. L. Williams, and G. Bowtell, “Self-propelled anguilliform swimming: Simultaneous solution of the two-dimensional Navier-Stokes equations and Newton’s laws of motion,” *J. Exp. Biol.* **201**, 3143 (1998).
- ³⁴S. Kern and P. Koumoutsakos, “Simulations of optimized anguilliform swimming,” *J. Exp. Biol.* **209**, 4841 (2006).
- ³⁵M. Gazzola, P. Chatelain, W. M. Van Rees, and P. Koumoutsakos, “Simulations of single and multiple swimmers with non-divergence free deforming geometries,” *J. Comput. Phys.* **230**, 7093 (2011).
- ³⁶C. Zhang, H. Huang, and X.-Y. Lu, “Free locomotion of a flexible plate near the ground,” *Phys. Fluids* **29**, 041903 (2017).
- ³⁷B. E. Griffith and N. A. Patankar, “Immersed methods for fluid–structure interaction,” *Annu. Rev. Fluid Mech.* **52**, 421 (2020).
- ³⁸R.-N. Hua, L. Zhu, and X.-Y. Lu, “Locomotion of a flapping flexible plate,” *Phys. Fluids* **25**, 121901 (2013).
- ³⁹G. Liu, Y.-L. Yu, and B.-G. Tong, “Flow control by means of a traveling curvature wave in fishlike escape responses,” *Phys. Rev. E* **84**, 056312 (2011).
- ⁴⁰G.-J. Dong and X.-Y. Lu, “Characteristics of flow over traveling wavy foils in a side-by-side arrangement,” *Phys. Fluids* **19**, 057107 (2007).
- ⁴¹Q. Zou and X. He, “On pressure and velocity boundary conditions for the lattice Boltzmann BGK model,” *Phys. Fluids* **9**, 1591 (1997).
- ⁴²J. C. Svendsen, J. Skov, M. Bildsoe, and J. F. Steffensen, “Intra-school positional preference and reduced tail beat frequency in trailing positions in schooling roach under experimental conditions,” *J. Fish Biol.* **62**, 834 (2003).
- ⁴³E. Akoz and K. W. Moored, “Unsteady propulsion by an intermittent swimming gait,” *J. Fluid Mech.* **834**, 149 (2018).
- ⁴⁴M. Hultmark, M. Leftwich, and A. J. Smits, “Flowfield measurements in the wake of a robotic lamprey,” *Exp. Fluids* **43**, 683 (2007).
- ⁴⁵T. Y. Wu, “Fish swimming and bird/insect flight,” *Annu. Rev. Fluid Mech.* **43**, 25 (2011).
- ⁴⁶A. P. Maertens, A. Gao, and M. S. Triantafyllou, “Optimal undulatory swimming for a single fish-like body and for a pair of interacting swimmers,” *J. Fluid Mech.* **813**, 301 (2017).
- ⁴⁷M. Gazzola, M. Argentina, and L. Mahadevan, “Scaling macroscopic aquatic locomotion,” *Nat. Phys.* **10**, 758 (2014).